Effect of thermal treatment on mechanically deformed cobalt powder

A. S. Bolokang[ab], M. J. Phasha[a], S. T. Camagu[a], D. E. Motaung[c], S. Bhero[b]

[a]Council for Scientific and Industrial Research (CSIR)
Materials Science and Manufacturing, Meiring Nude Rd, Brummeria, P.O. Box 395, Pretoria 0001, South Africa

[b]Department of Engineering Metallurgy, University of Johannesburg, P.O. Box 17011, Doornfontein 2028, South Africa

[c]DST/CSIR Nanotechnology Innovation Centre, National Centre for Nano-structured Materials, Council for Scientific Industrial Research, P. O. Box 395, Pretoria, 0001, South Africa

Abstract

Stabilization of the FCC phase was obtained after sintering the mechanically milled Co powder at 1400^{o}C. The Co powder retained its HCP crystal structure after MM. Phase identification on the milled and sintered Co powders was performed by the X-ray diffraction analysis, while morphology and microstructures were performed using both optical and scanning electron microscopy. Phase transformation traced by the differential scanning calorimetry.

1. Introduction

Synthesis of metastable phases in transition metals by using several non-equilibrium processes such as mechanical milling (MM) [1-4], cold pressing (CP) [5], and water quenching (WQ) [6] have attracted a huge interest in engineering and materials science. For many years, these non-equilibrium techniques were employed on metallic alloys, but for the last decade, an effort to study pure metals has increased. In the current investigation, the authors decided to focus on a ferromagnetic commercially pure fine cobalt (Co) metal. Cobalt (Co) is one of the vital transition metals used in electronics

and magnetic recording [7]. It exists in FCC, HCP or HCP/FCC in small, large and mixture of grains depending on the processing technique of the metal [8,9]. When subjected to MM, Co transform from HCP to FCC phase [10-13], similarly around 330 to 417 ^{o}C when thermally treated [14]. Apart from the metastable FCC allotropic phase transformation, there are studies reporting the metastable BCC crystal structure obtained in Co films [15, 16]. The stabilization of BCC Co depends on the crystalline size range of 2 to 5 nm [17]. In cemented carbides, Co is a suitable binder for HCP WC particles processed via powder metallurgical route. In is the modern trend that nanocrystalline powders are used to improve the strength of cemented carbides [18-20]. Therefore, alloyed nanocrystalline carbide powders have been synthesized using MM technique [21, 22], while in cases where only particle refinement is needed, Co is added to promote lower sintering temperatures [23]. When added with other pure metals during MM, Co XRD intensity peaks disappear in the early stages of milling [23, 24]. In the previous investigations, MM of Co, W, V and C powders has resulted in the formation of a new complex, Co-rich carbide structure upon sintering [25]. Furthermore, it is known that excess Co, W and C yields eta phase formation, that are detrimental to the overall mechanical properties during sintering of WC-Co cermets [28-30]. Investigations into the thermal behaviour of pure metals processed via MM might help to clarify many of the complex properties of metastable phases in alloys and compounds. In the current study, we focus on characterization of commercially pure Co powder, before milling and after MM and their thermal stability.

2. Experimental Work

In this work, Co powder of 99.8 % purity was used. This pure Co powder charge was milled under argon atmosphere at milling speed of 250 rpm for 10 h. Milling was performed in the stainless steel milling medium consisting of 5 mm diameter balls and vial at ball-to-powder ratio of 10:1. Milling vial was equipped with cooling system to avoid heating during milling. A small powder

sample was used for crystal structure analysis and morphology. Unmilled, milled and mixture of unmilled and milled powders were cold pressed at a pressure of 20 MPa to form cylindrical compacts of 17mm in diameter and 2 mm in thickness. These compacts were sintered in a Xeron vacuum furnace at temperature of 1400^{o}C for 1 hour. The sintered Co compacts were cross-sectioned for microstructural analysis using Leica DMI 5000M optical and LEO 1525 field-emission scanning electron microscope (FE-SEM coupled with a Robinson Backscatter Electron Detector (RBSD) and an Oxford Link Pentafet energy dispersive x-ray spectroscopy (EDX) detector. Phase evolution was traced with a Phillips PW 1830 X-ray diffraction (XRD) machine fitted with Cu Kα radiation, and 0.02 step size scanned from 20^{o} to 90^{o} (2θ). In order to determine the milled powder crystallite size, the Scherrer formula (Eq. (1)) was used from the full width at half maximum (FWHM) of the most intense Bragg peak.

$D=k\lambda/\beta_{hkl}\cos\theta_{hkl}$.....1

k=0.9, λ=0.154056 nm where: θ=diffraction angle, D=crystallite size,

λ= X-ray wavelength, B full width at half maximum (FWHM).

The Microtac Bluewave particle analyzer was employed to determine the particle size of unmilled and milled Co powders. Thermal analysis was carried out using DSC and TG incorporated in NETZSCH STA. Samples were heated up to 900 °C with Al_2O_3 as a baseline. A heating rate of 20 °C min^{-1} under argon gas at 20 ml/L standard flow rate was used. The macro-hardness measurements were carried out using FV-700 Vickers hardness tester with 2 Kg load

3. Results and Discussions

3.1 Powder characterization

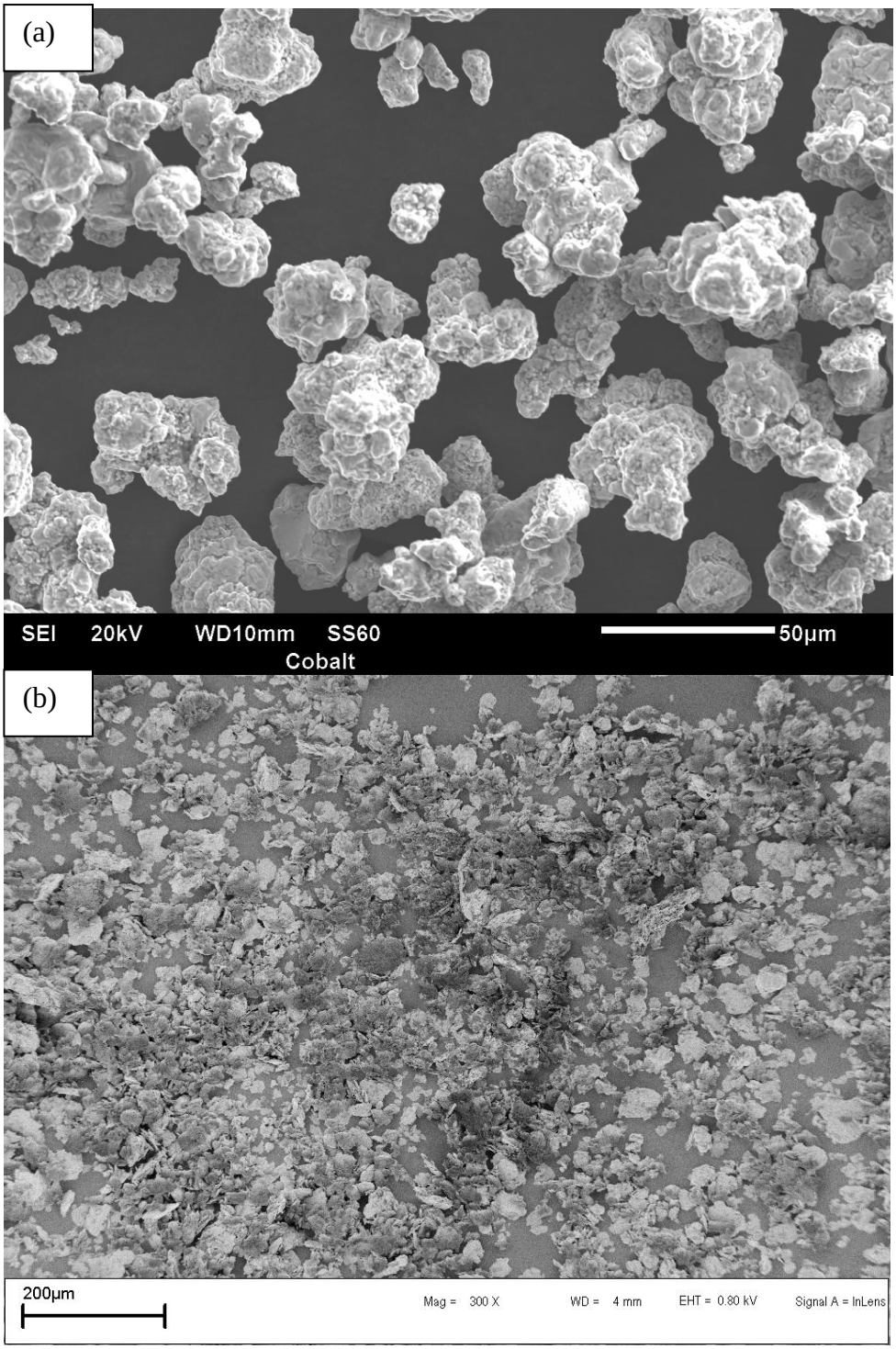

Figure 1: SEM Micrographs of (a) unmilled, (b) 10 h milled cobalt powders

Figure 1 (a) shows the SEM powder morphology of unmilled Co. The unmilled Co powder resembles an irregular popcorn shape that seems to be agglomerates of fine particles. In Figure 1 (b), it is evident that powder particles become thin and small after milling. The particle size analysis displayed in Table 1 confirms the reduction. Unmilled particles diameter for cumulative 10 (D_{10}), 50 (D_{50}) and 90 (D_{90}) weight per cent are 19, 32, 52, and 11, 29, 39 μm for 10 h milled respectively. Generally, the D_{10}, D_{50} and D_{90} for the 10 h mechanically milled powder show a decrease in particle sizes.

Table 1: Particle size distribution of Co unmilled and MM powders

Powder (μm)	D_{10}	D_{50}	D_{90}
Unmilled	19	32	52
10 h milled	11	29	39

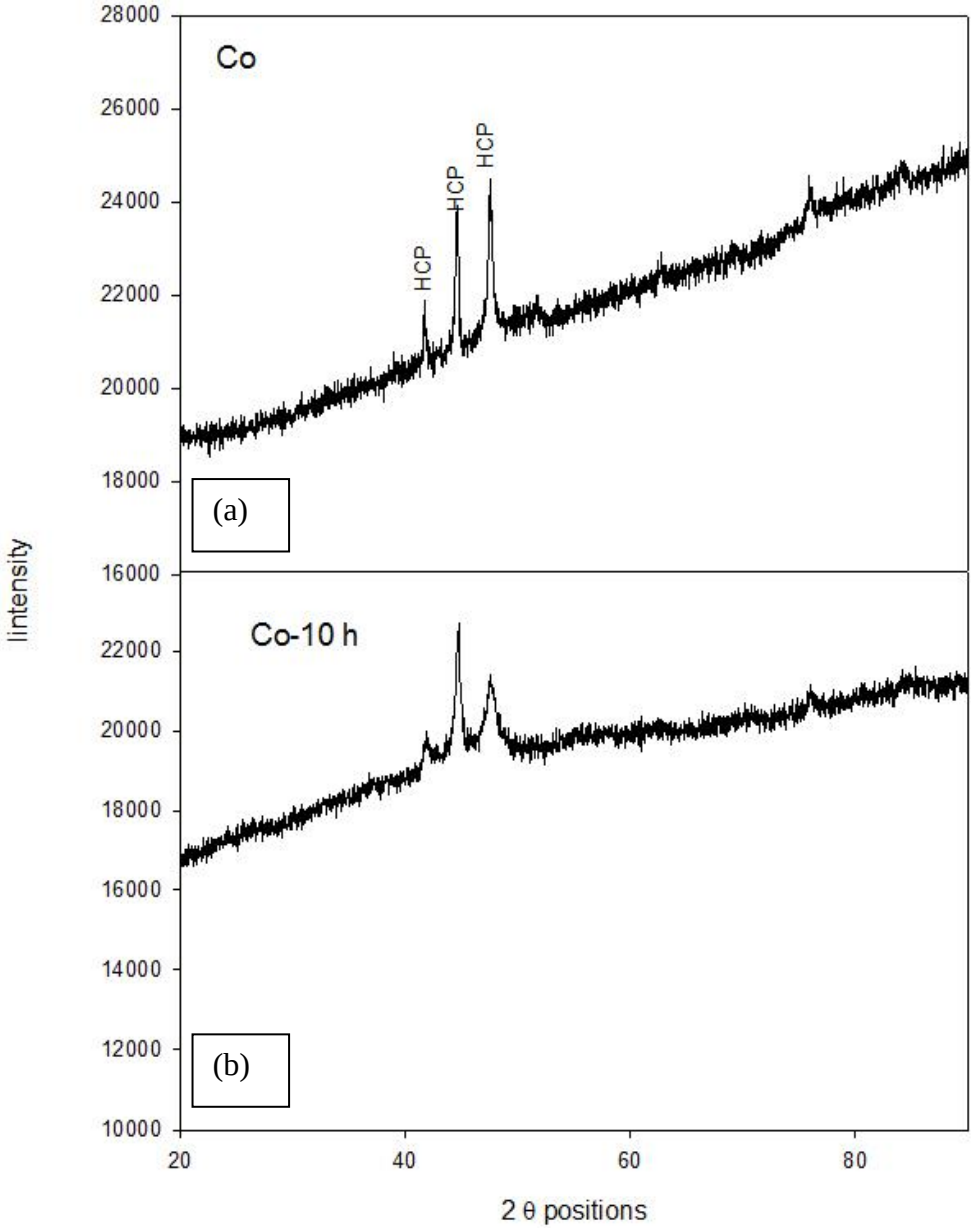

Figure 2: XRD pattern of (a) unmilled and (b) MM Co powders

In Figure 2 (a) and (b), the XRD patterns of unmilled and milled Co powders are shown. The pattern of the unmilled Co XRD spectrum resembles the behaviour of amorphous materials [31-33] or amorphous nanoparticles [34]. There are three main peaks of HCP while other remaining peaks illustrate an amorphous behaviour not in similar appearance than the ones observed on other reported unmilled Co powders [10, 11]. XRD pattern of unmilled Co makes a steep curve when compared to that of 10 h MM pattern. It became evident that the steep behaviour improves after MM probably due to

crystallinity caused by thin flakes of welded fine particles induced during mechanical deformation, but even after MM the powder remains a mixture of nanocrystalline and amorphous. The estimated crystalline size calculated using Sheerrer equation show that 8 and 25 nm were obtained on unmilled and milled powders, respectively. The increase in crystalline size is attributable to welding of fine powder particles, hence our current results agree with the previous studies that showed amorphous to crystalline in alloys is induced by MM [35,36]. It should also be highlighted in the current study that, powders are acquired based on the particle size and purity, but processing of Co powder can yield varying properties. It is shown in the current study that, although the cobalt powder of micron-particle size was used, it is actually agglomerates of fines.

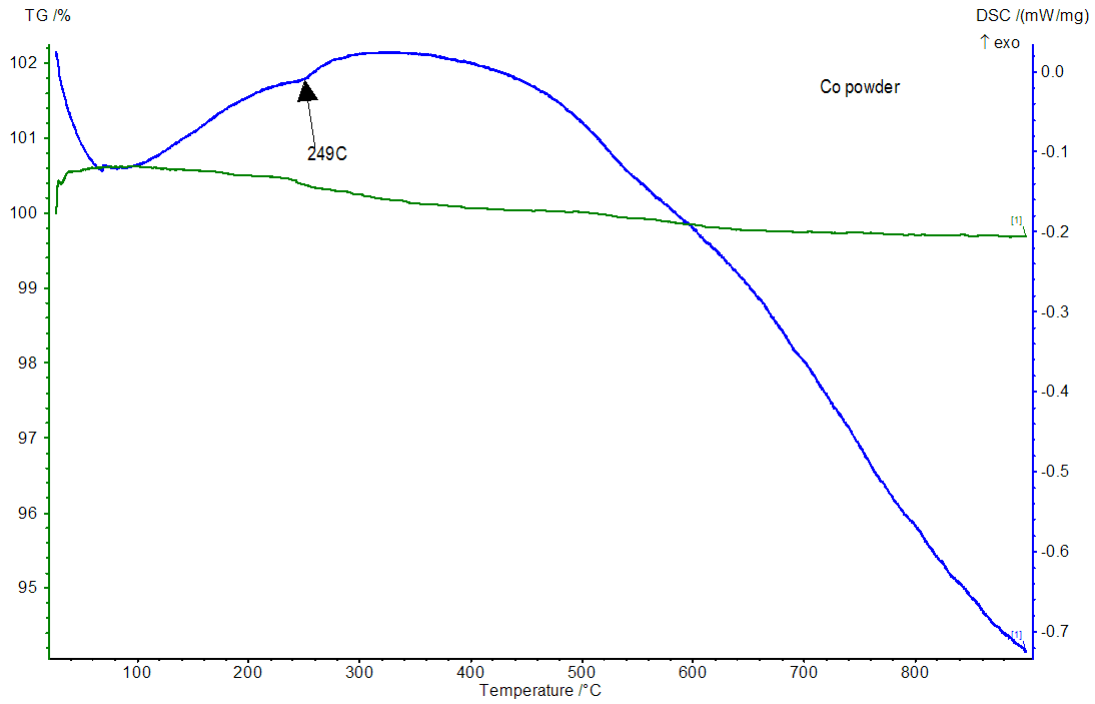

Figure 3: DSC-TG curve of unmilled Co powder

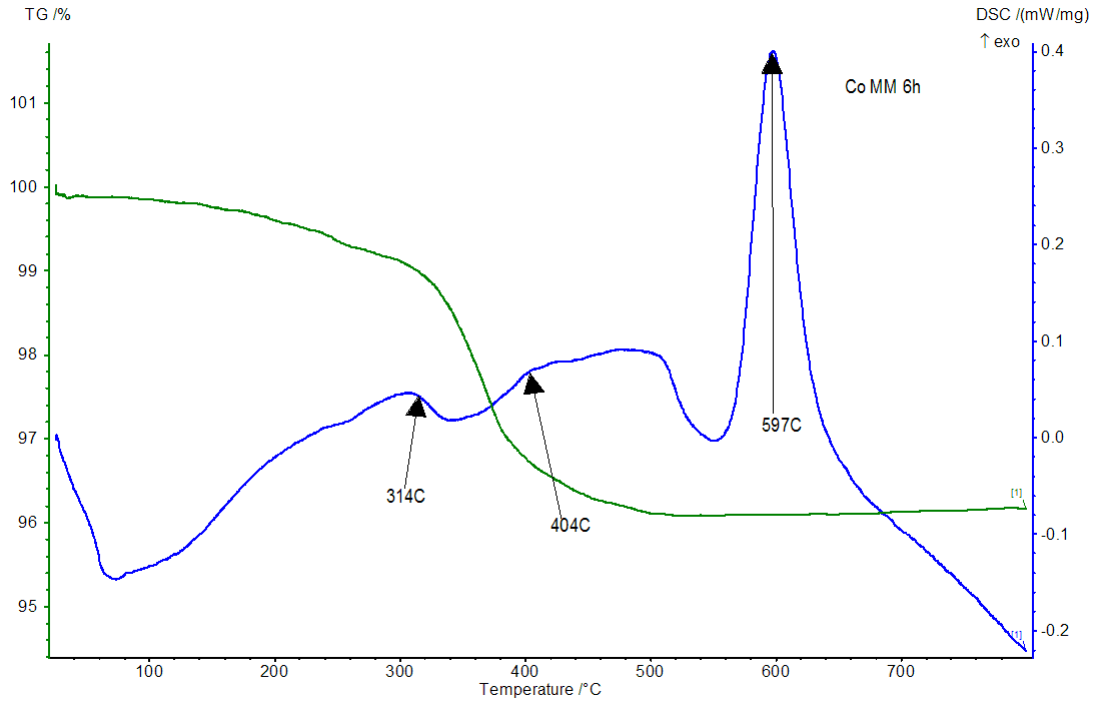

Figure 4: DSC-TG curve of 10 h mechanically milled Co powder

Figure 3 display a broad exothermic peak ending approximately at 500^{o}C during DSC-TG analysis of unmilled Co powder. This peak shows a stress relief, which is a confirmation of a highly stressed material. In addition to that, a small endothermic peak occurred at 249 ^{o}C, similar to what was shown on Xie et al amorphous material [34].To confirm the nature of such endothermic peak shown in Figure 3, unmilled powder was annealed at 550 ^{o}C for 30 minutes. It has emerged that the peaks is because of FCC transformation confirmed by the XRD analysis shown in Figure 5 (a). HCP phase was also retained upon annealing. The same endothermic has occurred on the milled powder in Figure 4. At this instance, the endothermic is broader and more distinct starting at 314 and ending at 404 ^{o}C. This FCC phase transformation (endothermic) peak is broad, distinct and starts to occur at 314 ^{o}C as shown in Figure 4. A well-defined endothermic peak support that small particles were welded to improve crystallinity. In addition, a sharp exothermic peak at 597^{o}C attributable to crystallization of the remaining amorphous phase has emerged. In Figure 3 and 4, the TG curves do not show any gain in weight. The indication of weight loss as shown by the

corresponding TG curve in Figure 4, rules out the possibility of oxidation. Weight loss may be due to volume expansion during heating [37]. Any oxidation or compound formation shows the increase in weight [38]. In order to validate the development of milled powder structure during thermal analysis, annealing was done at 650 ^{o}C above the crystallization exothermic peak. The XRD analysis in Figure 5 (b) reveals the presence of a single FCC phase after annealing. Large particles surface area of the thin flakes induced by mechanical deformations is attributed to the FCC stabilization.

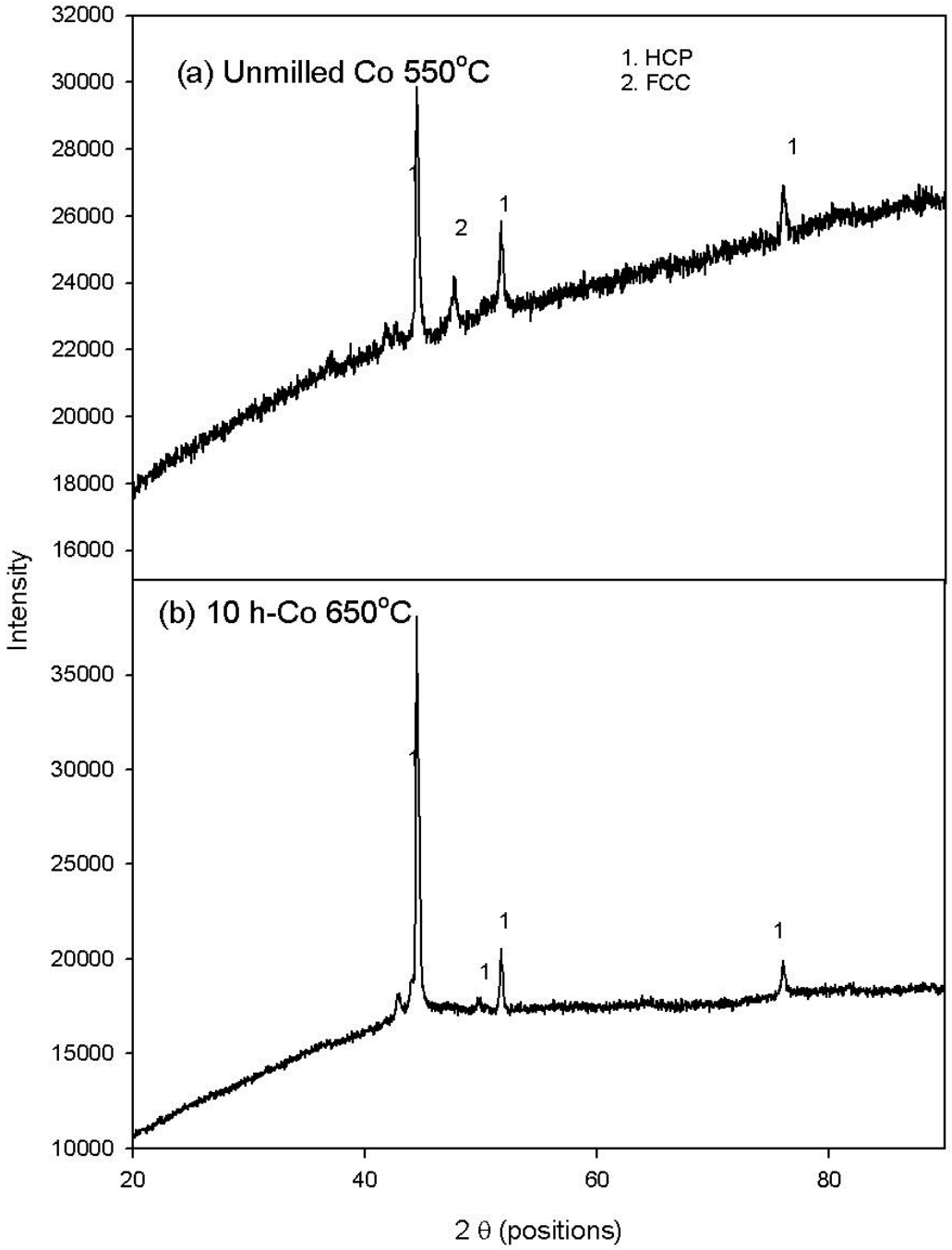

Figure 5: XRD patterns of annealed (a) unmilled and (b) mechanically milled Co powders.

3.2 Sintering

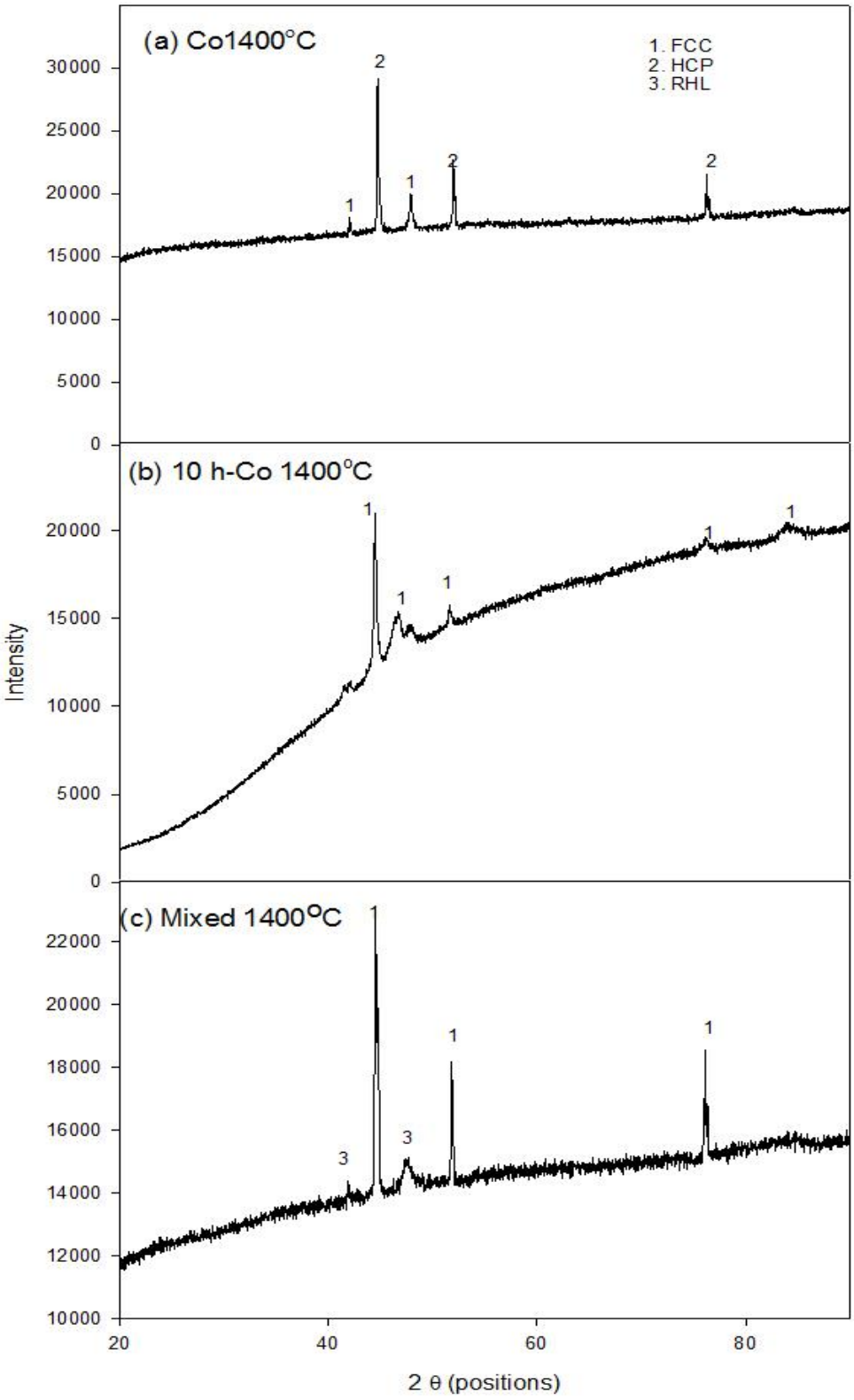

Figure 6: XRD patterns of sintered (a) unmilled, (b) 10 h milled and (c) mixture of milled and unmilled Co powders compacts.

To investigate the thermal stability, structure and mechanical properties of both unmilled and milled Co powders, we have sintered compacts at 1400^{o}C. In figure 6 (a) to (c), the XRD patterns of sintered Co compacts are presented. Figure 6 (a) shows that HCP and FCC phases were retained after sintering, similar to the annealed unmilled powder in Figure 5 (a). It was assumed that the FCC phase is attributable to smaller grains, while HCP is due to larger grains after sintering [8, 9]. The XRD pattern of the compact made from 10 h mechanically milled powder in Figure 6 (b), yielded a single FCC phase after sintering. Despite the calculated crystalline size of 25 nm after milling as compared to 8 nm for unmilled powder, the stabilization of FCC phase was obtained after sintering. Our results indicate that FCC phase in Co is induced not only from crystalline refinement during MM, but milling also activates its stabilization during thermal treatment because of deformation stresses induced on HCP Co structure. The FCC phase does not revert to HCP after sintering at 1400^{o}C. Therefore, deformation stress induced after MM makes FCC phase favourable upon thermal treatment. It is expected that only upon melting of powder that HCP phase can be recovered. To explore further the properties Co powder, we prepared a mixture of equal weight amounts of milled and umilled powder and subject them to sintering. The phases of FCC and rhombohedral structures were identified. It seems, although both individual powder compacts has only FCC and HCP, a rhombohedral crystal orientation was preferred. The lattice parameters of phases formed are presented in table 2.

Table 2: XRD properties of Co, MM 10 h, and mixed at 1400^{o}C

Temperature (^{o}C)	*Space group & number*	Phases	Lattice Parameter (Å)	
			a	*c*
Unmilled powder	P63/mmc # 194	HCP	2.51	4.08
Milled Powder	P63/mmc # 194	HCP	2.51	4.07
Annealed Unmilled 550		HCP FCC	2.51 3.52	4.08 -
Annealed MM 650	Fm-3m#225	FCC	3.54	-

Sint 1400 (Unmilled)	P63/mmc # 194 Fm-3m #225	HCP FCC	2.51 3.54	4.09 -
sint 1400 milled	Fm-3m #225	FCC	3.54	-
Sint 1400 mixed	Fm-3m #225 R-3m#166	FCC RHL	3.52 3.82	 2.89

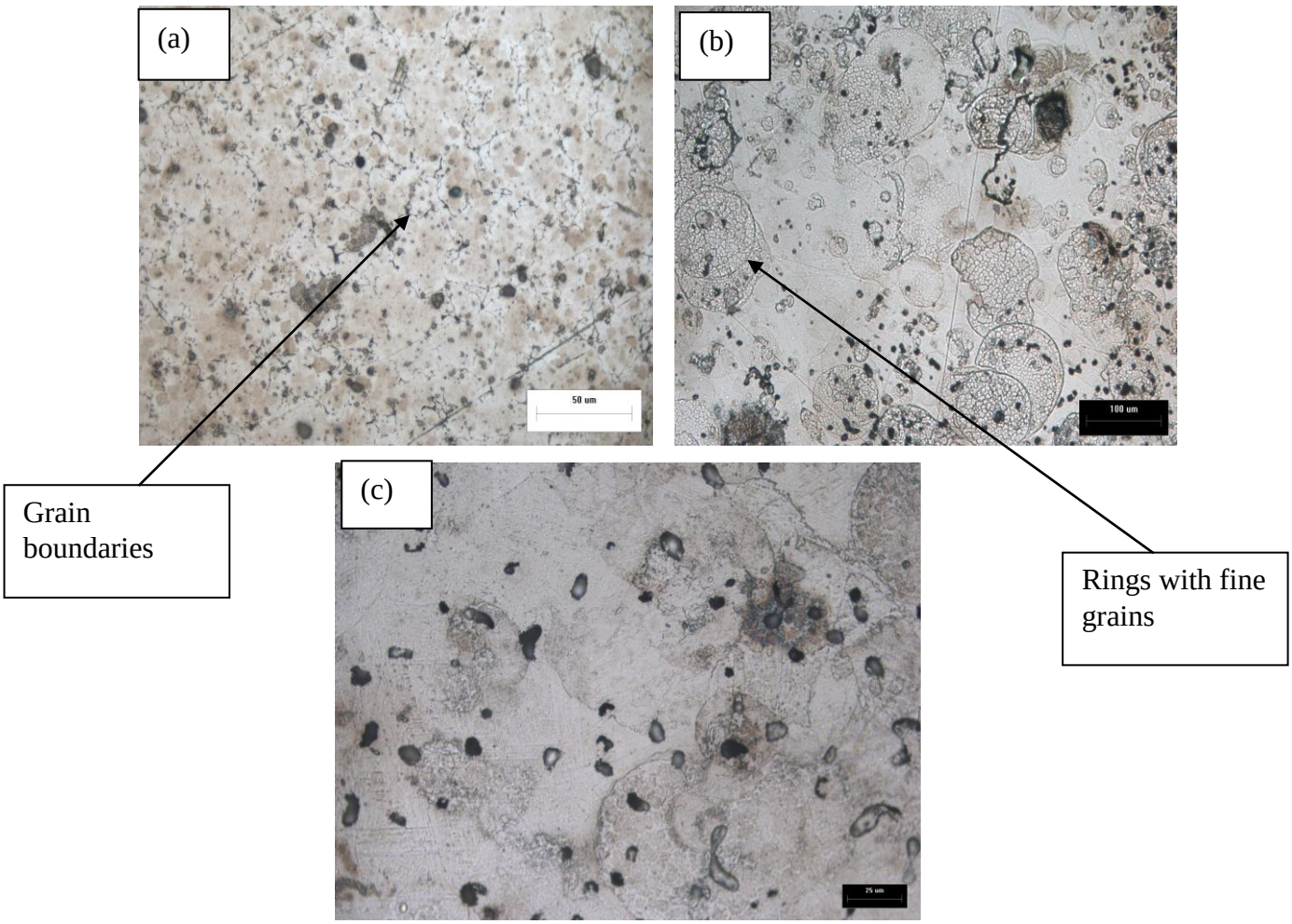

Figure 7: Optical micrographs of Co (a) unmilled, (b) milled and (c) mixed compacts sintered at 1400^{o}C viewed at 10X Magnification

The optical microstructures of sintered compacts are shown in Figure 7 (a) to (c) representing the unmilled, 10 h mechanically milled and mixture (unmilled and 10 h milled), respectively. Figure 7 (a) show evidence of small and large grain boundaries. The microstructure in Figure 7 (b) illustrates rings composed of small grain boundaries in a matrix. The high hardness of 300 VHN is attributed to the fine grains that are absent in Figure 7 (a) and (c). In

Figure 7 (a) and (c) the measured average hardness were 50 HVN and 130 HVN, respectively as shown in figure 9. The fine-grained structure obtained after sintering the milled powder has promoted high hardness and stabilization of FCC phase [8]. Karimpoor et al [39] have reported high strength in nanocrystalline Co, hence our result agrees to their findings. Figure 7 (c) show some similarities to the microstructure in Figure 7 (b) but its ring phases are not clear. It becomes apparent that the hardness of the milled sintered compact was significantly reduced upon addition of unmilled powder. Figure 9 display the statistical Vickers hardness curve of the sintered Co compacts.

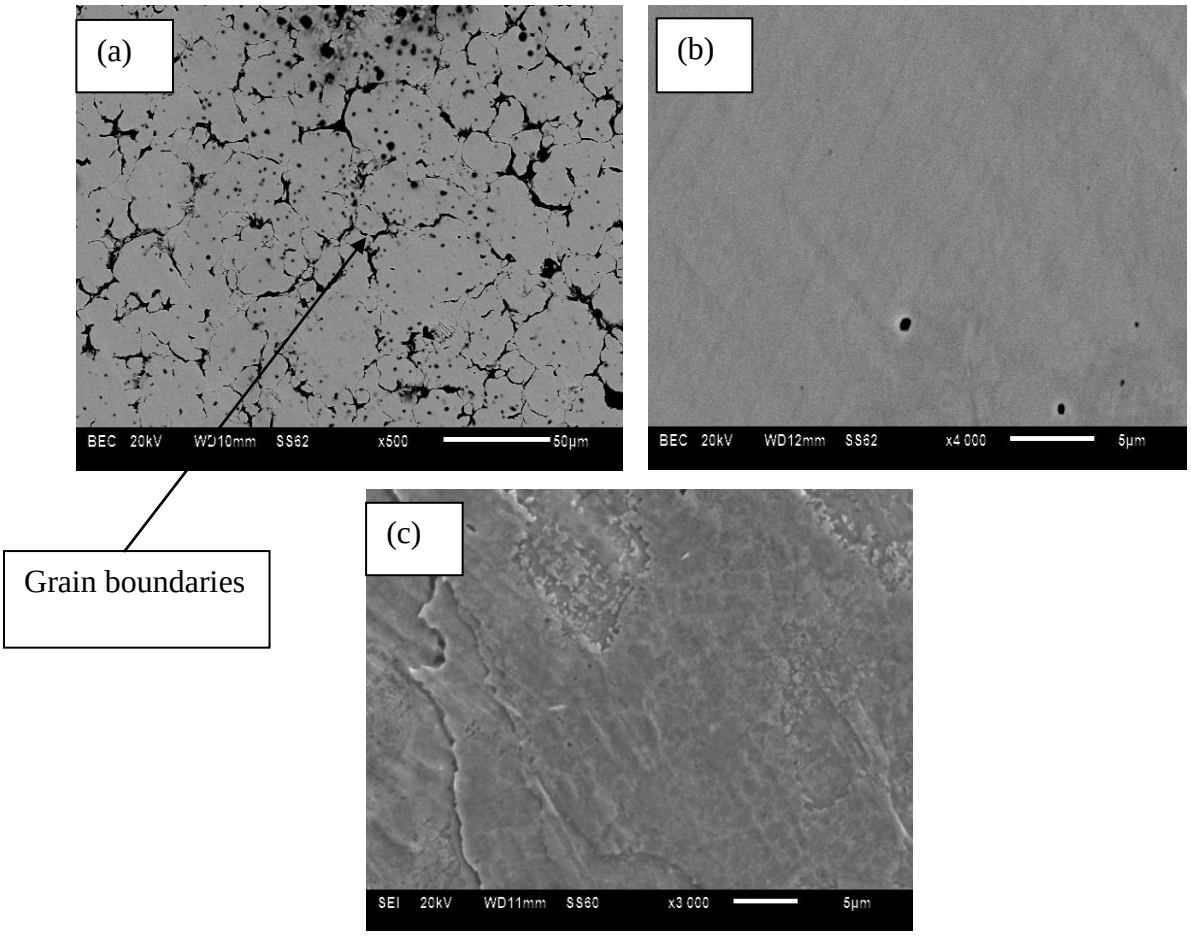

Figure 8: SEM micrographs of Co (a) unmilled, (b) milled and (c) mixed compacts sintered at 1400^{o}C

In figure 8 (a), the SEM micrograph of unmilled sintered compact is display a second phase (dark) on the grain boundaries, while in Figure 8 (b) and (c),

no distinct grain boundaries could be identified. Compositional analysis performed by using the EDS could not detect any form of contamination on all the sintered materials. Therefore, the metstable phases obtained in Co encourage the current authors to assume that the formation FCC Co-contained phases [20, 25-28], rhombohedral [40], and amorphous structures [36, 41-43] are due to influence of such metastable phases in pure Co.

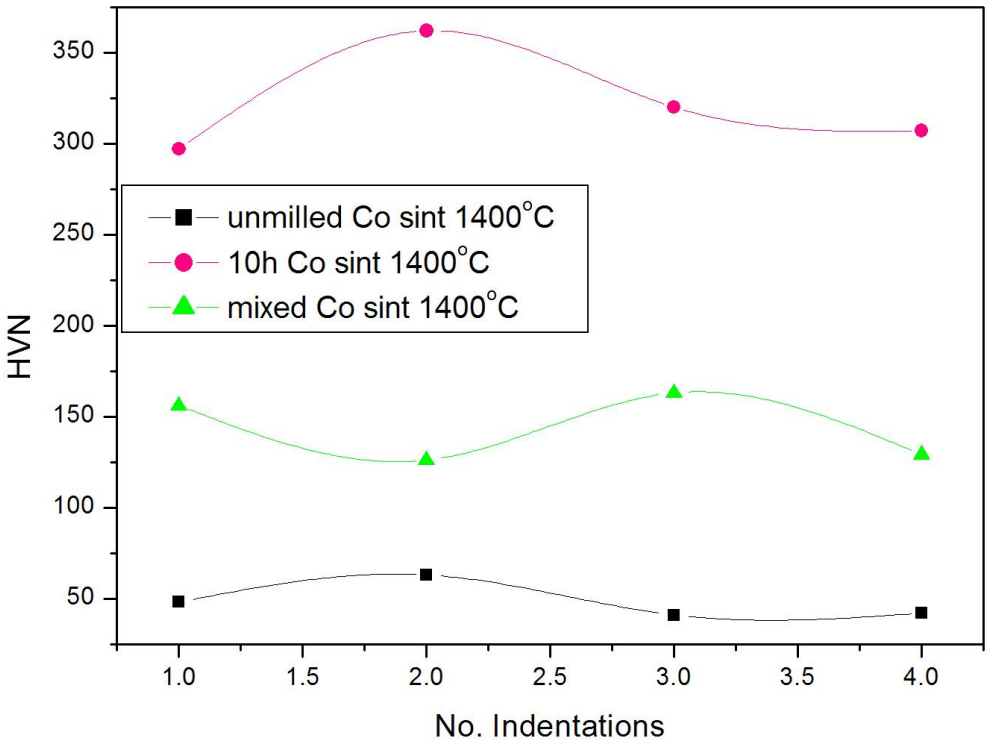

Figure 9: Vickers hardness graph of unmilled, milled and mixed Co

4. Conclusions

Characterization of unmilled powder showed that agglomerates of fine and amorphous Co particles [34] might exist as micron-sized particles. MM of Co powders for 10 h has changed the irregular, porpcon-type into HCP thin plate shapes. Annealing and sintering of these thin flakes and compacts has induced single FCC phase transformation. The DSC analysis show an endothermic FCC phase transformation peak that is broad, distinct and starts

occurring at higher temperature (314 ^{o}C) than that in of unmilled Co (249 ^{o}C). Due MM sharp exothermic peak at 597^{o}C due to crystallization of the amorphous phase follows has emerged. Annealing of the milled powder at 650 ^{o}C proves the formation of FCC phase, detected by the XRD analysis. The FCC phase became stable and did not revert to HCP after sintering at 1400^{o}C. After sintering of the unmilled powders, HCP and FCC were obtained. The mixture unmilled and milled yielded FCC and rhombohedral phases, respectively. The microstructure of mechanically milled and sintered compacts has the hardness of 300 VHN on average, larger than 50 VHN and 130 VHN unmilled and mixture, respectively. MM on Co powder activates the stabilization of metastable FCC during thermal treatment.

5. Acknowledgements

This work was supported by the Department of Science and Technology (DST) of South Africa and the Council for Scientific and Industrial Research (CSIR), division of Materials Science and Manufacturing (MSM) in the Metals and Metals Processing (MMP) unit.

6. References

[1] Manna I, Chattopadhyay PP, Nanadi P, Banhart F, Fecht HJ. Formation of face-centered-cubic titanium by mechanical attrition. J Appl Phys 2003;93:1520-4.

[2] Chattopadhyay PP, Pabi SK, Manna I, A metastable allotropic transformation in Nb induced by planetary ball milling. Mater Sci Eng A 2001; 304-306:424-8.

[3] Phasha MJ, Bolokang AS, Ngoepe PE, Solid-state transformation in nanocyastalline Ti induced by ball milling. Mater Lett 2010;64:1215-8.

[4] Chatterjee P, Sen Gupta SP. An X-ray fiffraction study of nanocrystalline titanium prepared by high-energy vibrational ball milling. Appl Surf Sci 2001;182:372-6.

[5] Karin A, Bonefacic A, Duzevic D. Phase transformation in pressed cobalt powder. J Phys F:Met.Phys 1984;14:2781-6.
[6] Bolokang AS, Phasha MJ. Novel synthesis of metastable HCP Ni by water quenching. Mater Lett 2011;65:59-60
[7] Pileni MP. Mesoscopic domains of cobalt nanocrystals. Pure Appl Chem 2002;74:1707-18.
[8] Owen E.A, Madoc Jones D. Effect of grain size on the crystal structure of cobalt. Proc Phys Soc B 1954; 67:456-66.
[9] Kajiwara S, Ohno S, Honma K, Uda M. A new crystal structure of pure cobalt in ultrafine particles. Philos Magazine Lett 1987;55:215-9.
[10] Huang JY, Wu YK, Ye HQ, Lu K. NanoStructured Mater 1995;6:723-6.
[11] Sort J, Nogues J, Surinach S, Baro MD. Microstructural aspects of the hcp-fcc allotropic phase transformation induced by ball milling. Philosophical Magazine 2003;83:439-55.
[12] Sort J, Nogues J, Surinach S, Munoz JS, Baro MD. Correlation between stacking fault formation, allotropic phase transformations and magnetic properties of ball-milled cobalt. Mater Sci Eng A 2004;375-377:869-73.
[13] Delogu F. Kinetics of allotropic phase transformation in cobalt powders undergoing mechanical processing. Scripta Mater 2008;58:126-9.
[14] Matsumoto H. Variation in transformation hysteresis in pure cobalt with transformation cycles. J Alloys Compd 1995;223:1-3.
[15] Spiridis N, Slezak T, Zajac M, Korecki J. Ultrathin epitaxial bcc-Co films stabilized on Au)001)-hex. Surf Sci 2004; 566-568:272-7.
[16] Idzerda YU, Elam WT, Jonker BT, Prinz GA. Structure determination of metastable cobalt films. Phys Rev Lett 1989;62:2480-3.
[17] Ram S. Allotropic phase transformations in HCP, FCC and BCC metastable structures in Co-nanoparticles. Mater Sci Eng A 2001;304-306:923-7.
[18] Fang Z, Maheshwari P, Wang X, Sohn HY, Griffo A, Riley R. An experimental study of the sintering of nanocrystalline WC-Co powders. Int J Refract Met Hard Mater 2005;23:249-57.

[19] Ou XQ, Song M, Shen TT, Xiao DH, He YH. Fabrication and mechanical properties of ultrafine grained WC-10Co-0.45Cr_3C_2-0.25VC alloys. Int J Refract Met Hard Mater 2011;29:260-7.
[20] Enayati MH, Aryanpour GR, Ebnonnasir A. Production of nanostructured WC-Co powder by ball milling. Int J Refract Met Hard Mater 2009;27:159-63.
[21] Wang GM, Campbell SJ, Calka A, Kaczmarek WA. Synthesis and structural evolution of tungsten carbide prepared by ball milling. J Mater Sci 1997;32:1461-7.
[22] Bolokang S, Banganayi C, Phasha M. Effect of C and milling parameters on the synthesis of WC powders by mechanical alloying. Int J Refract Met Hard Mater 2010;28:211-6.
[23] Xueming MA, Gang JJ. Nanostructured WC-Co alloy prepared by mechanical alloying. J Alloys Compd 1996;245:30-2.
[24] Bolokang AS. A comparison of the mechanically alloyed (V,W)C and (V,W)C-Co powders. J Alloys Compd 2009;477:905-8.
[25] Bolokang AS, Phasha MJ, Oliphant C, Motaung D. XRD analysis and microstructure of milled and sintered V, W, C, and Co powders. Int J Refract Met Hard Mater 2011;29:108-11.
[26] Allibert CH. Sintering features of cemented carbides WC-Co processed from fine powders. Int J Refract Met Hard Mater 2001;19:53-61.
[27] Ban ZG, Shaw L L. On the reaction sequence of WC-Co formation using an integrated mechanical and thermal activation process. Acta Materialia 2001;49:2933-9.

[28] Suetin DV, Shein IR, Ivanovskii AL. Structural electronic and magnetic properties of η carbides (Fe_3W_3C, Fe_6W_6C, Co_3W_3C and Co_3W_3C) from first principles calculations. Physica B 2009;404:3544-9.

[29] Menendez E, Sort J, Concustell A, Surinach S, Nogues J, Baro MB. Microstructural evolution during solid-state sintering of ball-milled nanocomposite WC-10 mass % Co powders. Nanotechnology 2007;18:1-9.

[30] Li C-J, Ohmori A, Harada Y. Effect of powder structure on the structure of thermally sprayed WC-Co coatings. J Mater Sci 1996;31:785-94.
[31] Calka A, Wexler D, Oleszak D, Bystrzycki J. Formation of amorphous and nanostructural powder particles from amorphous metallic glass ribbons using ball milling and electrical discharge milling. Solid State Phenomena 2005;101-102:111-6.
[32] Zhou GF, Bakker H. Atomically disordered nanocrystalline Co2Si by high-energy ball milling. J Phys Condens Matter 1994;6:4043-52.
[33] Koltypin Y, Katabi G, Cao X, Prozorov R, Gedanken A. Sonchemical preparation of amorphous nickel. J Non-crystalline Solids 1996;201:159-62.
[34] Xie C, Hu J, Wu R, Xia H. Structure transition comparison between the amorphous nanosize particles and coarse-grained polycrystalline of cobalt. Nanostructured Mater 1999;11:1061-6.
[35] Birol Y. Crystallization of a $Fe_{36}Ni_{36}B_{28}$ metallic glass during ball-milling. Scripta Mater 1996;34:1081-5.
[36] Bednarcik J, Kovac J, Kollar P, Roth S, Sovak P, Balcerski J, Polanski K, Svek T. Crystallization of CoFeSiB metallic glass induced by long-time ball milling. J Non-Cryst Solids 2004;337:42-7.
[37] Bolokang AS, Phasha MJ. Thermal analysis on the curie temperature of nanocrystalline Ni produced by ball milling, Advanced Powder Technology (2010), doi:10.1016/j.apt.2010.07.005
[38] Bolokang AS, Phasha MJ. Formation of titanium nitride produced from nanocrystalline titanium powder under nitrogen atmosphere. Int J Refract Met Hard Mater 2010;28:610-5.
[39] Karimpoor AA, Erb U, Aust KT, Palumbo G. High strength nanocrystalline cobalt with high tensile ductility. Scripta Mater 2003;49:651-6.
[40] Gupta KP. The Co-Mo-W system (Cobalt-Molybdenum-Tungsten). J Phase Equilidria 2002;23:274-7.
[41] Louidi S, Bentayeb W, Sunol JJ, Mercier AM, Greneche JM. Amorphization of Cr-10Co mixture by mechanical alloying. J Non-Cryst Solids 2010;356:1052-6.

[42] Grabchikov SS, Yaskovich AM. Effect of the structure of amorphous electrodeposited Ni-W and Ni-Co-W alloys on their crystallization. Russian Meatllurgy 2006;2006:56-60.
[43] Sheikholeslam MA, Enayati MH, Raessi K. Characterization of nanocrystalline and amorphous cobalt-phosphorus electrodeposits. Mater Lett 2008;62:3629-31.